SUPPLEMENTARY INFORMATION

1 Characteristics of Region of Interest

Galactic centre region defined In this work we define the Galactic centre (GC) region to be an elliptical region of 3° semi-major axis (along the Galactic plane) and 1° semi-minor axis, centred on the Galactic dynamical centre (corresponding to physical scales of ~ 420 pc and ~ 140 pc at the assumed GC distance of 8 kpc). This region easily encompasses the Central Molecular Zone[29], the agglomeration of dense molecular matter along the Galactic plane within ~ 200 pc of the actual GC that represents up to 10% of the Galaxy's H_2 allocation (a total mass approaching $10^8\ M_\odot$[30]) and corresponds, more or less, to the usual definition of the Galaxy's Nuclear Bulge[30]. In previous work[31] the diffuse but discrete region of non-thermal radio emission around the Galactic centre investigated here has been labelled the 'diffuse non-thermal source' or DNS.

Volume of the diffuse non-thermal source We assume the diffuse non-thermal source emission volume to be an elliptical spheroid with circular cross-section in the Galactic plane (i.e., its greatest line-of-sight extent is equal to its width along the plane). This implies a total volume of $\sim 3.0\times10^{63}$ cm^3.

Gas filling factors We have derived the filling factors (for molecular gas at the various number densities investigated) from a study of the density distribution of molecular gas throughout the GC (see fig. 6 of [32]) and the total hydrogen gas mass contained within the diffuse non-thermal source over its assumed volume, viz. $\sim 3 \times 10^7\ M_\odot$ (accurate to a factor ~ 2 [30]).

We note that, discounting all the gas at densities greater than 1000 cm^{-3}, the diffuse non-thermal source volume contains $\sim 2.4\times10^6\ M_\odot$ of relatively low density molecular hydrogen, with

rather similar amounts of atomic hydrogen (HI) and 'warm' ionized hydrogen (H^+). The presence of these phases imply a minimum (path-integrated) n_H for a diffuse non-thermal source electron of ~ 2.7 cm^{-3} (The putative 'very hot', plasma phase of the Galactic nuclear bulge, that would have a filling factor of $\sim 85\%$, would have lower number density than this. However, relativistic electrons will not be trapped in this phase[33].)

As briefly stated in the main article there is an on-going debate in the literature about the reality of this 8 keV plasma – some researchers[34] have long argued that the apparently diffuse emission is actually due to unresolved, faint X-ray sources. We emphasise that while our argument for a 100 μG field is consistent with the existence of a diffuse 8 keV plasma it does not require it and our argument for the magnetic field lower bound at 50 μG holds regardless of whether the plasma is real or not.

Velocity dispersion of molecular gas The internal velocities of GC molecular clouds span the range 15–30 km/s[[35]] . This is consistent with the mean line width found in a study[36] of GC molecular clouds of 22.8 km/s.

2 Observational material and methods

Sources of radio data for our diffuse non-thermal source radio spectrum are listed in table 1. As an historical aside, we note that large-scale radio emission around the Galactic Centre region is evident in radio maps produced at least as early as 1964[37]. Historically important surveys at 5 GHz were published in 1971[38] and 1973[39] but we have not had access to these data. (We emphasise this is certainly not an exhaustive list.)

In addition to the radio data employed in the paper, in table 1 we also list 8.35 and 14.35 GHz data[44]. Unfortunately, the data at these frequencies were processed with a median filtering algorithm that artificially attenuates the flux density of sources larger than $\sim 34'$ so that these flux densities represent lower limits. Note that the 14.35 MHz datum shows the expected[46] up-break

ν (GHz)	Telescope	Beam ($'$)	Flux density (Jy)	Error	Reference
.074*	VLA	2	16,200 Jy	1,000 Jy	31
.330†	Green Bank	39	18,000	5%	31
.330‡	VLA	2	1,000	-	31,40
1.408	Effelsberg	9.4	7,300	10%	41
2.417	Parkes	10.4	4,900	6%	42
2.695	Effelsberg	4.3	4,400	10%	43
8.35**	Green Bank Earth Station	9.7	1,300	5.6%	44
10.29	Nobeyama	2.9	1,400	7%	45
14.35**	Green Bank Earth Station	6.6	1,200	8.3%	44

Table 1: Surveys and Observational data used to derive the spectrum for the $6^\circ \times 2^\circ$ region centred on the GC. Notes: *At 74 MHz the large-angle Galactic plane synchrotron background/foreground flux contribution is not measured (and hence not accounted for) due to the interferometric nature of the VLA observation. †Total flux (measured with Greenbank single dish) supplied by Dr Crystal Brogan (private communication). ‡Flux attributable to discrete sources $< 1^\circ.2$. **Lower limit.

above 10 GHz due to the rising contribution from spinning dust (the 14.35 GHz lower limit is, therefore, not adopted as a constraint in our fitting). The full radio spectrum including the 8.35 and 14.35 GHz lower limits is shown in figure S1.

In addition to the radio maps at 74 MHz and 330 MHz presented elsewhere[31] and the convolved 10 GHz map shown in the main paper, we show below the diffuse non-thermal source radio

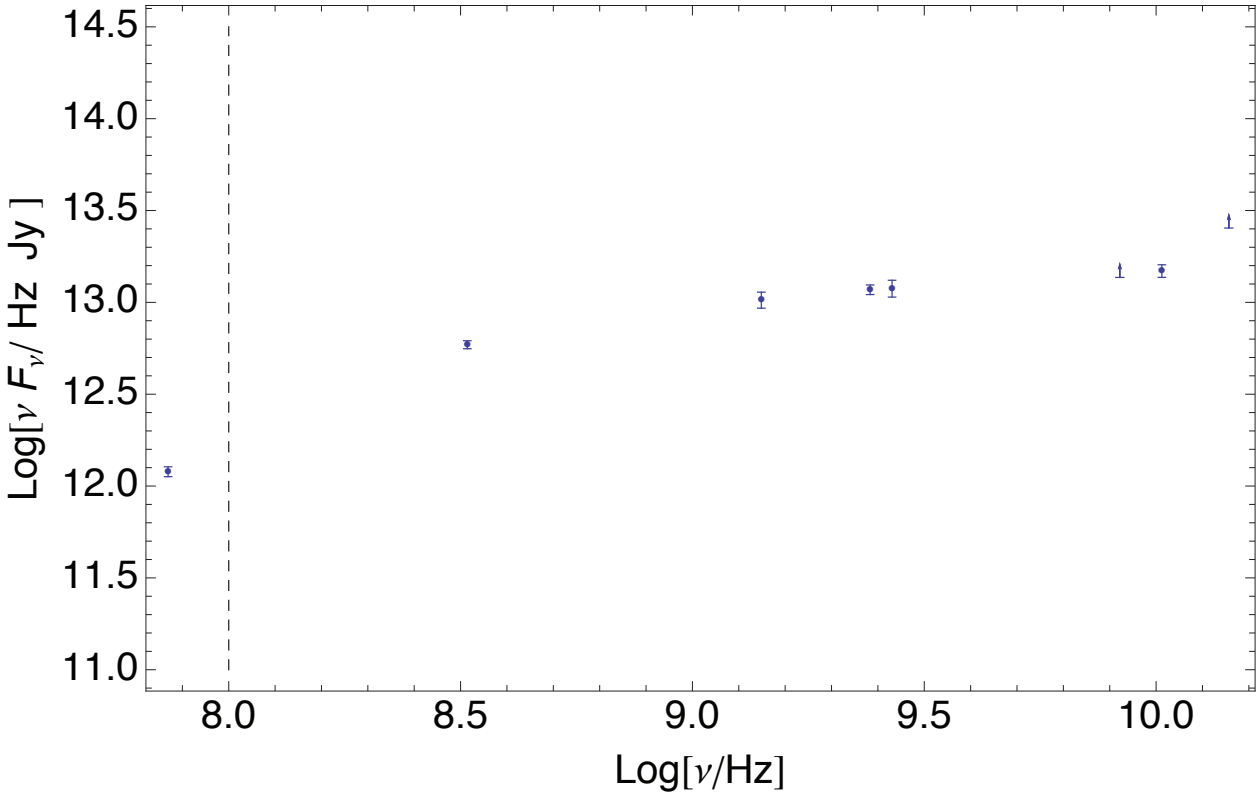

Figure S1: **The raw diffuse non-thermal source radio spectrum**. The vertical dashed line divides the 74 MHz datum (that does not include a contribution from the Galactic plane synchrotron background/foreground due to the interferometric nature of the VLA observations) from all the other data (that do). This creates the artificial impression of a break at ∼300 MHz. The real break is at ∼GHz. The 8.35 and 14.35 GHz flux densities are actually lower limits[44]. Above 10 GHz the spectrum becomes dominated by emission from spinning dust[46] and the 14.35 GHz lower limit is not employed, therefore, as a constraint in our fitting.

maps at 1.408, 2.417 and 2.695 GHz in both native resolution and convolved versions (the latter to emphasis the large amount of large-angle diffuse emission in the field). The 2.695 GHz map does not give full coverage of the diffuse non-thermal source. On the basis of the 2.417 GHz map, the region inside the diffuse non-thermal source ellipse and to the west of $l = -2^\circ$ (*not* mapped at 2.695 GHz) is relatively dim with respect to the rest of the diffuse non-thermal source. To deal with this problem we measure the average intensity inside the diffuse non-thermal source and to the east of $l = -2^\circ$ at this frequency and then weight this intensity *downwards* by the ratio of the 2.417 GHz intensity over the entire region to the 2.417 GHz intensity excluding the region to the west of $l = -2^\circ$. This amounts to a correction at the $\sim$5% level. This corrected 2.695 GHz is then multiplied by the solid angle of the entire diffuse non-thermal source ellipse to arrive at a total flux density datum at 2.695 GHz.

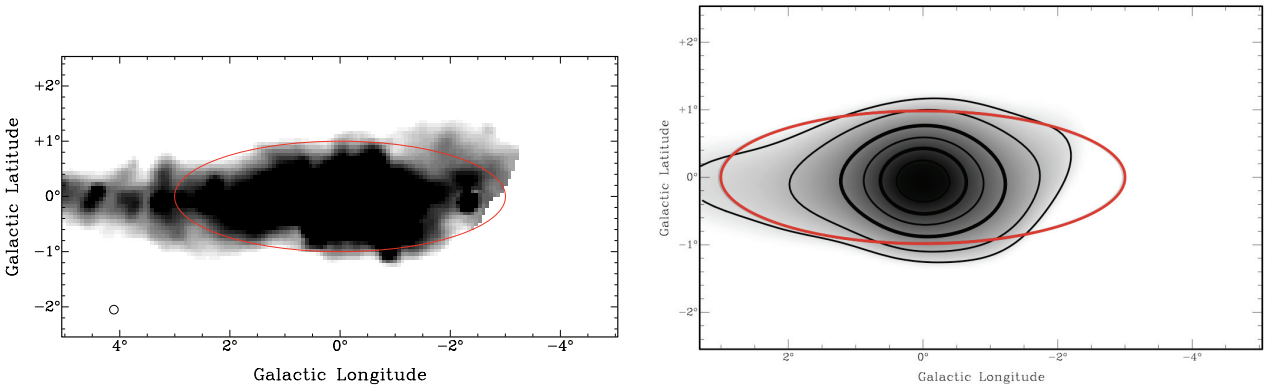

(a) Native resolution.

(b) Convolved to a resolution of $1^\circ.2 \times 1^\circ.2$. Contours at 25, 30, 40, 50, 60, and 70 K.

Figure S2: **Total intensity images of the diffuse non-thermal source at 1.408 GHz.** Logarithmic transfer function employed to highlight low intensity emission. The apparent abrupt cessation of emission at Galactic longitude $\sim 3^\circ$ is non-physical and simply reflects the limit of the survey.

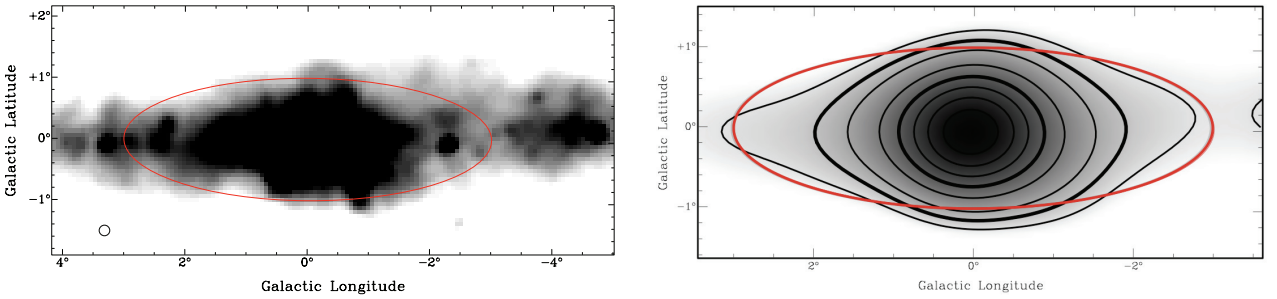

(a) Native resolution.

(b) Convolved to a resolution of $1^\circ.2 \times 1^\circ.2$. Contours at 425, 500, 600, 800, 1000, 1200, 1400 and 1600 Jy/beam.

Figure S3: **Total intensity images of the diffuse non-thermal source at 2.417 GHz.** Logarithmic transfer function employed to highlight low intensity emission.

Radio backgrounds and foregrounds As noted in the text there are two important sources of background and foreground radio emission for which we have to account: discrete sources (which include both optically thick and thin thermal sources and non-thermal sources) and the Galactic plane synchrotron background (GSB). To deal with these we follow a two step procedure: The first step is to low-pass filter the images (to account for discrete sources), the second is then to subtract an offset to account for Galactic synchrotron in front of or behind the Galactic center. We detail these steps below.

1. Discrete source background (or foreground): Previous investigations[31] measured a $\sim$ 1000 Jy flux density at 330 MHz attributable to discrete sources with the VLA[40]. These measurements were performed in an array configuration sensitive to emission out to a scale of $\sim 1^\circ.2$ at

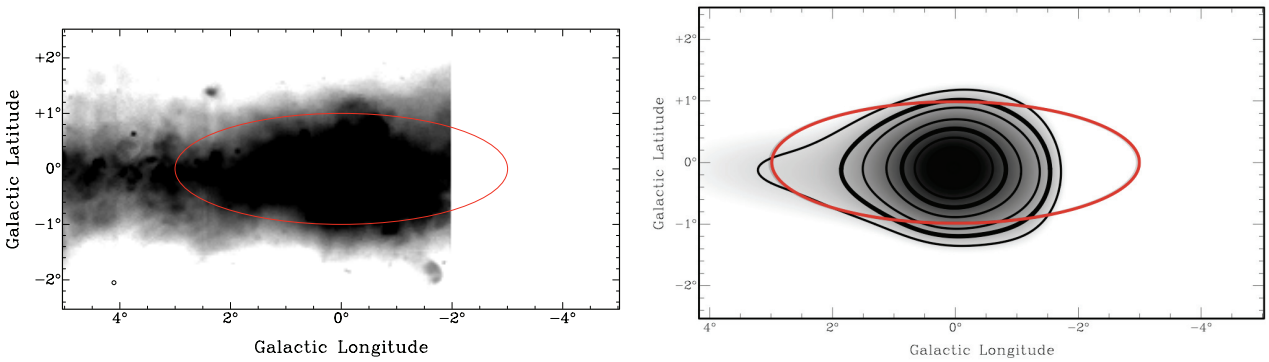

(a) Native resolution.

(b) Convolved to a resolution of $1^\circ.2 \times 1^\circ.2$. Contours at 4, 5, 6, 8, 10, 12, and 14 K.

Figure S4: **Total intensity images of the diffuse non-thermal source at 2.695 GHz.** Logarithmic transfer function employed to highlight low intensity emission.

this frequency. (One notes that the authors[40] conservatively only claim sensitivity out to an angular scale of 45', but we have checked in an independent reanalysis that the data are sensitive out to the larger $\sim 1^\circ.2$ angular scale: see below.) We have used a technique based on Fourier decomposition[47,48] (described below) to determine the flux density contribution of discrete sources up to this same angular scale for the higher-frequency, single dish data. In other words, we take flux densities from the single-dish data at the same wavenumber (of 50) where the Fourier spectrum of the VLA data flattens off to its limiting value of 1000 Jy – see Fig. S6. Including emission out to angular scales of $\sim 1^\circ.2$ within our discrete source background is highly conservative and, in particular, will capture almost all thermal emission, even that due to extended, low density HII regions[49]. The discrete source spectrum describes a power-law with a spectral break of ~ 0.2 at ~ 2 GHz. This moderate break (cf. the break in the discrete source subtracted data of $\sim$0.6) indicates that, given the conservatively-large scale of $1^\circ.2$ up to which "discrete" emission is con-

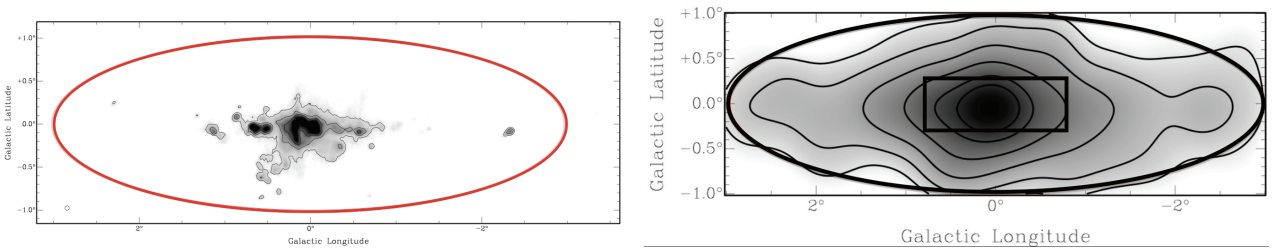

(a) Native resolution.

(b) Convolved to a resolution of $1^\circ.2 \times 1^\circ.2$. with contours at 10, 20, 40, 80, 160 and 240 Jy/beam.

Figure S5: **Total intensity images of the diffuse non-thermal source at 10.29 GHz.** Logarithmic transfer function employed to highlight low intensity emission.

sidered to originate (for consistency with previous work [31]), we still capture a contribution from the same cooled, non-thermal electron population identified in the diffuse flux density (viz., a broken power-law synchrotron-emitting electron population). That the break is much less than $\frac{1}{2}$, however, is consistent with our also capturing contributions from truly discrete sources in the field that are a combination of non-thermal, optically thick free-free ($\alpha = 2$ with $I_\nu \propto \nu^\alpha$), and optically thin free-free ($\alpha = -0.1$) emitters (as previously observed[50] at 5 and 8.5 GHz for a smaller field).

2. Line-of-sight Galactic plane synchrotron background/foreground: we have normalized the Galactic plane synchrotron background/foreground at 408 MHz via recourse to a previous Galactic plane survey[51] and, following previous work[31], chose a constant longitude slice free of discrete sources (well outside of the diffuse non-thermal source) near $l = 354^\circ.5$ to measure the latitude dependence of the 408 MHz flux density normalization. At higher frequencies we expect the Galactic plane synchrotron background/foreground to have a spectral index of $\alpha = -0.70 \pm 0.12$[52] (with $I_\nu \propto \nu^\alpha$). Note that the Galactic plane synchrotron back-

ground/foreground is expected to display a break at a frequency of $\sim$ 22 GHz[53], well above the region where we are fitting.

As we cannot directly measure the Galactic plane synchrotron background/foreground at higher frequencies due to the presence of other backgrounds, we emphasise that the Galactic plane synchrotron background/foreground spectral index is left as a free parameter in our fitting.

Method–Fourier Analysis: Radio interferometers such as the Very Large Array (VLA) filter out radiation emitted on scales larger than that representing the angular scale of the smallest baseline separation of two antennae at a given wavelength. Such emission is not recovered in image deconvolution. (It is for this reason that it is common practice, when imaging structures on large scales, to add back the information filtered out by the interferometer using single-dish data[54].)

The limiting outer angular scale (in radians) to which an interferometer is sensitive at a given wavelength λ is given by λ/b, where b is this (smallest) baseline. For the VLA operating at 330 MHz and using the most compact configuration (with a shortest baseline of 45 metres) this angular scale is 0.02 radians, in agreement with the angular scale quoted on the VLA official website[1] of $4200''$. Hence the $\sim$ 1000 Jy of flux density previously estimated[31] at 330 MHz is obtained from an angular scale of $\sim 4200''$. As remarked elsewhere, our own rendering of the visibility function of the previously-obtained VLA data confirms that the Fourier spectrum of these data levels off to $\sim$1000 Jy at a wavenumber of $\sim$50 (see solid line displayed in Fig. S6), corresponding to an angular scale of 0.02 radians or $1^\circ.2$.

[1] http://www.vla.nrao.edu/astro/guides/vlas/current/node9.html

In order to construct the radio spectrum of the diffuse non-thermal source – incorporating data obtained at different frequencies and with different instruments – we used the following algorithm:

1. The single-dish (and the interferometric 330 MHz VLA) data were regridded and convolved to the grid and resolution of the lowest-resoluation data (the Parkes 2.4 GHz data with beam $10.4'$).

2. The location of the central pixel in all images was changed to that corresponding to (*l,b*)=(0,0) for all images.

3. Each image was divided by the number of pixels per beam using the MIRIAD task *maths*, so that each pixel is rendered into Jy/pixel. The number of pixels per beam was calculated by dividing the beam area ($A_b = 1.133(\Omega_a \times \Omega_b)$) by the area of each pixel, where all units are in arcseconds.

4. The MIRIAD task *fft* was then used to take the Fourier transform of every image. The units of the Fourier transform of the intensity in Jy/pixel is in Jy[48]. The Fourier transform on each image was performed with the image in the sky plane (hence the Fourier transform performs a transform into the *uv*-plane). This means that data is transformed *after* any image weighting has (possibly – though not by us) been performed.

5. The MIRIAD task *ellint* was used to measure the average flux density in annuli of increasing radius (but constant thickness) from the centre of the (*u,v*)-plane

6. The discrete source flux density in the image at each frequency (all flux density on scales $< 1^{\circ}.2$) is then the flux density at a wavenumber of 50 in Figure S6.

Figure S6 shows a plot of flux density in Jy, against wavenumber for all the single-dish images at $\nu \geq 1.4$ GHz together with the 330 MHz VLA data. This shows that the emission at all size-scales follow a rough power law. In support of the validity of this technique as an estimate of the flux density as a function of angular scale, we note a couple of properties of this plot. Firstly, in the limit of wavenumber approaching zero we determine flux densities from the FA technique that agree within better than 3% with those obtained by directly integrating the total flux density in the diffuse non-thermal source at each frequency (after re- gridding and convolution to the PKS 2.4 GHz image). Additionally, the flux density at a wavenumber of 50, which corresponds to the outer angular scale of the VLA using the 330 MHz data[40] matches the flux density that we have found using the unsharp masking technique[55]. Thus we believe that rather than being representative of the RMS flux density from the region, the FA flux densities derived here represent the total flux density within the region. We also note that at all angular scales under consideration the emission is non-thermal (clearly the average spectrum flattens towards high wavenumbers/small angular scales consistent with the expectation of an increasingly relative contribution from optically thick and thin free-free emission).

As a final confirmation of our technique, we observed the GC region with the Australia Telescope Compact Array at 1.384 and 2.368 GHz in the 750 A and D configurations (with angular sensitivity matched to that of the VLA at 330 MHz in the C and D configurations used in previous

observations[31]). The mosaic maps we have produced at these frequencies do not cover the entire extent of the diffuse non-thermal source but do measure the brightest region (of extent $2^\circ \times 1^\circ$) along the plane. These measurements therefore proffer lower limits on the discrete source flux density contribution at ~ 1.4 and ~ 2.4 GHz which are ∼80 and 70%, respectively, of the central values we have found using the Fourier-decomposed single dish data (see fig. 2 or the main article).

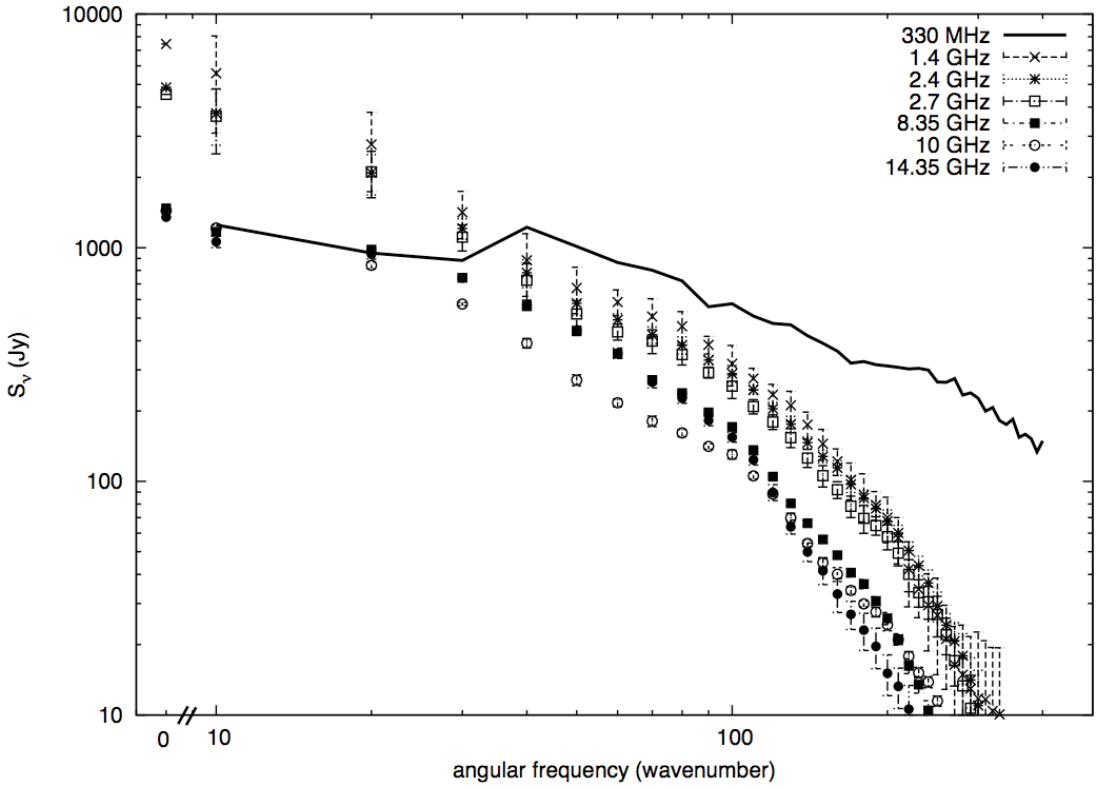

Figure S6: **Flux as a function of wavenumber for the $\nu \geq$ 1.4 GHz single dish data (data points) and the 330 MHz VLA (interferometer) data (solid line)**. The limiting outer scale out to which the VLA is sensitive (at 330 MHz and in its compact configuration) is shown to correspond to a wavenumber of ∼50 (an angular scale of $\sim 1/50 = 0.02$ radians $\simeq 1.2^\circ$

Errors The errors for all radio flux densities in this paper (as given in table 1) have been determined as follows:

1. The 74 MHz datum has an error for the *total* diffuse non-thermal source flux density of 1000 Jy[31].

2. At 330 MHz, we adopt an error of 5%[50].

3. We assume 10% errors at 1.4 and 2.7 GHz, since these images adopt absolute zero measurements from previous 408 MHz images[51] and 10% is nominated as the systematic error in the latter.

4. At 2.4 GHz we adopt 6% from a previous study[56] involving observations of the same region with the same telescope but at 5 GHz. At 10 GHz we adopt an error of 7% from a previous study[57] involving observations of a different region, but at the same frequency and with the same telescope.

5. For the discrete source flux densities obtained from Fourier analysis of single-dish data, we obtained a conservative error estimate by choosing as large a region as possible that was below the Galactic plane, common to all maps, and containing no significant emission features (no discrete sources, little Galactic plane emisison). We derived the Fourier spectrum of this region at each frequency to estimate the amount of power in any given region attributable to RMS noise fluctuations. We scaled the total flux density at a wavenumber of 50 from the noise region by the relative size of the diffuse non-thermal source to give the error on the discrete source flux density.

74 MHz datum: We treat the 74 MHz flux density measured previously[31] as a datum in our fitting. The authors responsible for this measurement state that the 74 MHz flux formally represents a lower limit. We show here why we are justified in treating it as a datum to be fit in our modelling.

The flux density measured by the VLA over the diffuse non-thermal source at 74 MHz might be attenuated for any of the following reasons, which we address in turn.

1. **Interferometric nature of observation:** As mentioned above for the case of the 330 MHz observations by the VLA, there is a limiting outer angular scale to which an interferometer is sensitive, at a given wavelength. For the VLA operating at 74 MHz in the most compact configuration, the official VLA website[2] gives this scale as $20000''$ or $\sim 5.5^\circ$. This is slightly smaller than the largest extent of the diffuse non-thermal source structure, 6°. The diffuse non-thermal source structure is effectively divided into two[31], however, because of absorption by the discrete HII regions located along the line-of-sight near Galactic longitude 0° (see below). Moreover, our own rendering of the visibility function of the previously-obtained 74 MHz VLA data confirms that the flux density within the diffuse non-thermal source grows as an approximate power law for wavenumbers $\sim 500 \rightarrow \sim 12$ and that the extrapolation of this power law to a wavenumber of 9.5 (corresponding to an angular scale of 6°) predicts a flux density in agreement (to within 7%) of the flux density we find 'directly' within the diffuse non-thermal source (using the algorithm described above).

2. **Free-free absorption by discrete HII regions:** at low frequencies and along the Galactic

[2] http://www.vla.nrao.edu/astro/guides/vlas/current/node9.html

plane, radio flux density is attenuated by absorption within discrete HII regions located along the line-of-sight to the region of interest. There is no doubt that this process is affecting the diffuse non-thermal source observation at 74 MHz[31]. To correct for this bias, previous work[31] has not simply integrated within the boundary of the diffuse non-thermal source to arrive at a 74 MHz flux density, rather the "average 74 MHz flux density at locations within the diffuse non-thermal source that appear free of both discrete emission sources and thermal absorption, together with its apparent size (an ellipse of dimension $6^\circ \times 2^\circ$)"[31] has been used to calculate the total flux.

3. **Free-free absorption by a covering HII screen:** the only situation for which the above procedure could not compensate is if there were a diffuse, covering HII screen that presents a roughly constant emission measure over the entire diffuse non-thermal source (implying a minimum optical depth over the entire diffuse non-thermal source solid angle that could not be recovered). We deal with this possibility at length below and show that – given access to higher frequency data covering the same region – we can also dismiss it as a cause of attenuation.

HII screen? The effect of an HII screen covering the entire diffuse non-thermal source cannot be recovered by considering the 74 MHz data in isolation. An upper limit on the absorption by such a region may, however, be obtained by supposing that the flux density observed from the region *at some higher frequency* (for definiteness, 10 GHz where the spectrum reaches a minimum) is entirely explained by optically thin free-free *emission*. This follows as both free-free absorption

and emission can be related to the emission measure (i.e. the integral along the line of sight of the electron density squared). Then the free-free optical depth at 10 GHz is

$$\tau(10\ \mathrm{GHz}) = \frac{F(10\ \mathrm{GHz})}{\Omega_{DNS} B(10\ \mathrm{GHz}, T)} \tag{1}$$

where Ω_{DNS} is the solid angle subtended by the diffuse non-thermal source and $B(10\ \mathrm{GHz}, T)$ is the intensity of black body radiation of temperature T at 10 GHz. The formula above is valid only if $\tau(10\mathrm{GHz}) \ll 1$ (which is true over the reasonable range of parameters). We assume $T = 5000$ K[30]. So, if we take the most conservative assumption: the 10 GHz flux density is all free-free; we have all the information needed to get the free-free optical depth at 10 GHz, and having got it there, we can get it at any frequency ν:

$$\tau(\nu) = \tau(10\ \mathrm{GHz}) \left(\frac{\nu}{10\ \mathrm{GHz}} \right)^{-2.1}. \tag{2}$$

Then, assuming the synchrotron emission only suffers free-free absorption, the total flux density at frequency ν would be

$$F(\nu)^{tot} = F(\nu)^{syn} + F(\nu)^{freefree} \tag{3}$$

where

$$F(\nu)^{syn} = F(\nu)^{syn,0} e^{-\tau(\nu)}, \tag{4}$$

and

$$F(\nu)^{freefree} = \Omega_{DNS} B(10\ \mathrm{GHz}, T)[1 - e^{-\tau(\nu)}] \tag{5}$$

and $F_\nu^{syn,0}$ is the synchrotron flux density that would exist if there were no free-free absorption whatsoever[3].

[3]Note that an alternative to an HII screen would see a large-scale HII region *co-mingled* with the synchrotron-emitting phase of the diffuse non-thermal source volume. This case leads, however, to a smaller free-free optical depth

The essential question now is: can the effect of free-free absorption at 74 MHz on a pure power law synchrotron-emitting electron population (the null hypothesis case) produce the curvature we find in the diffuse non-thermal source radio spectrum (which we have interpreted as the bremsstrahlung to synchrotron cooling break)? To investigate this question numerically we allowed for a contribution to the (discrete source subtracted) total 10 GHz flux density from large-scale free-free emission with a corresponding amount of free-free absorption at 74 MHz (i.e., we produced a generalized model of the detected spectrum that accounts for free-free emission/absorption by a putative HII screen). With this extra parameter in the fitting (described in more detail below) we in fact find that a χ^2 analysis picks out a solution of vanishing free-free contribution to the (discrete source subtracted) total 10 GHz flux density, i.e., the best fit for the null hypothesis is obtained for the case of **no** all-over absorption of the 74 MHz flux density and this case presents, therefore, the most conservative supposition (i.e., any amount of absorption from a covering screen at 74 MHz implies more curvature in the intrinsic synchrotron spectrum because of the corresponding fraction of the total flux explained by free-free emission at 10 GHz) . In other words, we find that an HII screen cannot cause free-free absorption at 74 MHz in such a way that an intrinsically pure power law at emission is modified to imitate the spectrum we observe.

In summary, we arrive at a best-fit to the null hypothesis (of a pure power-law spectrum)

at 74 MHz for a given level of free-free emission at 10 GHz and it is, therefore, more conservative to assume a screen geometry. Also note that another logical possibility is for there to be many HII regions (presenting different emission measure) each individually only covering part of the diffuse non-thermal source. Again, however, this situation leads to less absorption *overall* (i.e., integrated over the entire solid angle) for a given amount of 10 GHz free-free emission and it is, therefore, appropriate to assume a covering HII screen of more-or-less uniform emission measure.

for the case of no all-encompassing free-free absorption (at 74 MHz) and emission (at 10 GHz). Our preferred model (of a cooled power law electron population) also favours no such absorption/emission. Together with the fact that we find the idea of such an all-over HII screen of any significant optical depth to be physically contrived, these results indicate that the 74 MHz flux arrived at previously[31] (after addressing points 1 and 2 above) is an actual measurement because either of the physically-reasonable models for the total emission requires negligible free-free emission (at 10 GHz) and absorption (at 74 MHz) by an all-over HII screen.

In any case, treating the datum in this way is conservative in the sense that the statistical difference between the null hypothesis and our model would be smallest were there no all-encompassing HII screen. From this point of view, taking the 74 MHz flux as a datum produces a lower limit on the statistical confidence with which our model can be accepted and the null hypothesis rejected. Altogether we are justified in adopting the 16,200 Jy flux density arrived at[31] (already corrected by them for discrete HII region absorption) as a datum (rather than a lower limit) in our analysis.

Fitting Procedure Our fitting of the radio data works as follows: the data to be fitted are i) the 74 MHz datum which already has the Galactic plane synchrotron background/foreground component pre-filtered out[31] given the interferometric nature of the VLA observations (sensitive out to a scale of $\sim 5.5^{\circ}$ degrees as described above) and ii) the remaining data which *do* include a Galactic plane synchrotron background/foreground contribution but *not* a discrete source contribution which has been measured (as described above) and removed at each frequency. We thus fit our model for

the signal (synchrotron emission from a cooled electron population governed by a power law in momentum *at injection*) *alone* to the 74 MHz datum whereas we fit the signal + Galactic plane synchrotron background/foreground to the remainder of the data. The floating fit parameters (the magnetic field is fixed for each trial) are the i) spectral index (we have constrained the range of injection spectral index to be $2.0 \leq \gamma \leq 2.4$ corresponding to the reasonable range that might be produced by first-order Fermi acceleration) and ii) normalization of the electron population at injection, iii) the ambient hydrogen number density, and (given we cannot directly measure the Galactic plane synchrotron background/foreground at higher frequencies due to the presence of other backgrounds) iv) the Galactic plane synchrotron background/foreground spectral index (the normalization of the Galactic plane synchrotron background/foreground is determined at 408 MHz as described above). We include a contribution from the fit-value of the Galactic plane synchrotron background/foreground spectral index to the total χ^2 (the spectral index of this background being Gaussian distributed around 0.695[52]). Therefore, the number of degrees of freedom (dof) for our main analysis is 3 (= 6 radio data points + 1 Galactic plane synchrotron background/foreground spectral index datum - 4 fit parameters). For the null hypothesis of a pure power law electron population, the n_H value is not a relevant parameter and $dof = 4$ (as described below we assume a minimum allowable $n_H \simeq 2.7$ cm^{-3} to calculate a conservative lower limit on bremsstrahlung emission for the null hypothesis case).

Fitting of synchrotron emission from cooled electron population Our calculational procedure – described at length elsewhere[58] – is performed within the 'thick target' regime wherein electrons are taken to cool *in situ* rather than escape via diffusion. That we are in this regime is guaranteed

by the fact that we *do* observe a break; free escape would imply an electron spectrum which is unmodified by injection. We note that a direct calculation, assuming that the electrons diffuse at the Alfven speed, confirms that the diffuse non-thermal source presents a thick target to electrons over the range of B and n_H we probe.

Robustness of Results In anticipation of a number of possible objections that might be raised against our analysis we note the following:

1. **We include *all* relevant cooling processes in our code**; ionization, bremsstrahlung, inverse Compton and synchrotron are all accounted for in arriving at the cooled electron distributions we investigate.

2. **Our analysis is not sensitive to the particulars of the discrete source removal**: a break is clearly seen in the data before removal of the discrete source contribution. In fact, the null hypothesis (of a pure power-law emitting electron population) provides a very poor fit to the data before removal of the discrete source flux density contribution (a reduced χ^2 of $\sim$9 for 3 dof excluded at $\sim$4.5σ).

3. **Our analysis is not sensitive to the particulars of the Galactic plane synchrotron background/foreground removal**: if, instead of fixing the Galactic plane synchrotron background/foreground flux density at the value we measure at 408 MHz, we allow it to be a free parameter (like the spectral index of this component) in our fitting, we find, e.g., for a magnetic field value of 100 μG a best-fit reduced χ^2 of 1.4 (for 3 dof) but the null hypothesis only achieves a best-fit reduced χ^2 of 3.7 (for 4 dof, acceptable only at the 2.8σ confidence

level) and this only for magnetic fields $\gtrsim 40\mu$G.

4. **10 GHz datum**: the evidence for the spectral break does hinge critically on the 10 GHz datum. We note, however, the following: if we do not effect the removal of small-scale flux density at 10 GHz and, instead, fit to the *total* radio flux density detected at this frequency, the null hypothesis provides, at best, a fit acceptable only at the 97% confidence level for a magnetic field $\gtrsim 50\ \mu$G.

5. **Alternative explanations for the break are not tenable:** this point deserves a detailed discussion which we present immediately below.

Alternative explanations for the break? Granted the reality of the break, there are four possible explanations for it including the mechanism explored in this paper. We show here that the other potential mechanisms do not work or – if they were true – they would lead to even larger estimates on the large-scale magnetic field than derived currently in our paper (so that assuming a synchrotron cooling break is the most conservative hypothesis). For the discussion below, note the following inputs: from the radio data directly, the break frequency is 1.7 GHz and the change in radio spectral index across the break is $\sim$0.6.

Potential explanations for the down-break in the diffuse non-thermal source radio spectrum:

1. A transition from bremsstrahlung to synchrotron cooling of the steady-state electron population as investigated in the paper. We take the opportunity to explain this mechanism for

the generation of a cooling break in a little more detail here. Such a break occurs when the dominant cooling process changes from bremsstrahlung emission (producing a cooling rate of $dE/dt \propto E_e \times n_H$ where n_H is the ambient hydrogen density) to synchrotron emission itself ($dE/dt \propto {E_e}^2 \times B^2$). This leads to a steepening of the cooled electron distribution by 1 in spectral index above the break energy, ${E_e}^{bk}$, where the two cooling rates are equal. The resulting synchrotron spectrum steepens by $\frac{1}{2}$ in spectral index above a frequency ν^{bk} corresponding to ${E_e}^{bk}$.

2. **A cut-off feature in the** *injected* **electron distribution:**. We can reject explanations of this type for the following reasons: i) they do not explain the change in spectral index of $\sim \frac{1}{2}$ which is *predicted* by the synchrotron cooling hypothesis and seen in the data, ii) hypothesising a cut-off in the *injection* spectrum this is required to be at $\sim$ GeV $(B/100\ \mu\mathrm{G})^{1/2}$ to reproduce the observed break at $\sim$ GHz. There is, however, direct evidence from the TeV observations by the HESS instrument of the Galactic centre[59] that – *within the same field* – acceleration/injection of electrons beyond a TeV is occurring. This conclusions follows irrespective of whether the observed diffuse TeV emission is due to inverse compton scattering by directly-accelerated electrons or to neutral pion decay following collisions of primarily accelerated *hadronic* cosmic rays (which latter would then imply injection of secondary electrons in large numbers well above 1 TeV).

3. **A non-steady state situation** where the break results from a transition from where (at lower energy) electrons have not had time to cool since an emission/injection/acceleration event to where (at higher energy) electrons **have** had time to cool. We label this scenario **synchrotron**

ageing.

A synchrotron ageing scenario requires a transition as we "scan" across the electron energy spectrum (from lower to higher energies): $t_{synch} > t_{age} \rightarrow t_{synch} < t_{age}$, where t_{age} is the time since a **single** emission/injection/acceleration event responsible for the relativistic electrons. To be in **non** steady state we would also require that $(t_{synch}, t_{age}) \ll t_{wait}$ where t_{wait} is the average time between emission/injection/acceleration events.

This can be quickly dismissed: a non steady state situation implies that the particles ultimately responsible for the radio emission diffuse over the entire diffuse non-thermal source over a timescale shorter than t_{wait}. Conservatively, the ultimate source of energy for the relativistic particles is supernova and, for the GC, we have conservatively, $t_{wait} \sim 10^4$ years (with 5-10% Galaxy's recent massive star formation occurring in the GC[60] one expects a SN every (10-20) $\times$ 100 yrs). Thus an unphysically large effective diffusion velocity, $v > c/3$ (given the 6° or 840 pc span along the Galactic plane of the diffuse non-thermal source emission region), is required in order that the system be out of steady state while, at the same time, synchrotron emission be observed emanating from the entire region.

In any case, even if a non-steady state situation pertained (despite the above reasoning) it would imply an even larger *lower* limit on the magnetic field strength than the scenario explored in the paper: solving for the unique combination of field amplitude and electron energy that give a break at 1.7 GHz due to synchrotron ageing (for $t_{age} = 10^4$ year), one determines a field amplitude of $\sim$2 mG. Even a t_{age} of 10^6 years implies a $\sim$100 μG field in order that a break be produced.

4. A steady-state situation where we see a transition from (at lower energies) particle **escape** (as distinct from *in situ* cooling) being the dominant loss process to (at higher energies) synchrotron (or inverse compton) cooling being the dominant loss process. We label this an "escape/cooling break".

   This is a steady state situation requiring $t_{esc} \sim t_{synch+IC}$ (where $t_{synch+IC} < 2 \times 10^7$ year), so the question here becomes: what is t_{esc}? Here we find two possibilities:

   (a) Escape is **advective** (via bulk motion of material entrained in a wind) which implies $t_{esc} \sim t_{wind}$, where t_{wind} is the (energy-independent) wind escape time. An upper limit on t_{wind} can be obtained by assuming that the particles stream out at the GC gravitational escape velocity which is 1000-1200 km/s[61]. Over the 1° or $\sim$140 pc semi-extent of the diffuse non-thermal source this implies a maximum wind escape time of 1.4×10^5 year. Again, solving for the field which implies a break at 1.7 GHz one finds a minimal field of 400 μG from this scenario.

   (b) Escape is **diffusive** which implies $t_{esc} \sim t_{diffsn}$, where $t_{diffsn} = r^2/(4D)$ is the diffusive escape time controlled by diffusion coefficient D from a region of size r. The energy dependence of D depends on the spectrum of magnetic turbulence responsible for scattering the charged particles under consideration. A lower limit on the diffusion coefficient is provided by the "Bohm" case for which $D \propto E$. This case is already ruled out as it leads to a diffusion (or confinement) time $\propto E^{-1}$, implying the injection spectrum of particles is steepened by 1 in spectral index – just as for synchrotron cooling which has exactly the same energy dependence (Bohm diffusion would, therefore,

not lead to a spectral downbreak). In fact, it is difficult to reconcile the observed break phenomenology with any diffusive loss scenario: the "Kraichnan" and "Kolmogorov" turbulence cases – typically invoked in the case of diffusion of Galactic cosmic rays – lead to energy dependences of the diffusion coefficients of $E^{1/2}$ and $E^{1/3}$, respectively. Energy-dependent confinement, therefore, steepens a particle injection spectrum by 1/2 and 1/3 in energy (again for the two cases of Kraichnan and Kolmogorov turbulence), transitioning to a steepening of 1 for the emitting electron spectrum when the synchrotron loss time becomes less than the diffusive escape time. This translates to a change in *radio* spectral index of only $1/2(1-1/2) = 1/4$ or $1/2(1-2/3) = 1/3$ for the Kraichnan and Kolmogorov cases. In contrast, the observed change in radio spectral index is $\sim$0.6 over the break.

Disregarding this issue, we still find that reasonable diffusive escape scenarios still imply stronger magnetic field lower limits than the synchrotron cooling hypothesis explored in the paper. We dopt the Galactic plane diffusion coefficient value quoted in a previous approach[59], viz $D = 10^{30}$ cm^2/s for 10 TeV protons diffusing through the Galactic plane. Accounting for the energy scaling of the diffusion coefficients, we have (solving for the field which produces a radio break at 1.7 GHz) for the Kolmogorov case, a minimum field of 450 μG and, for the Kraichnan case, a minimum field of 170 μG so that, again, the scenario of bremsstrahlung to synchrotron cooling explored in the paper is the more conservative.

Electron population energy density We have calculated the energy density of the non-thermal electron population assuming that it is governed by a power-law in *momentum* and integrate down to vanishing kinetic energy. If, instead, we integrate down to a kinetic energy equal to the electron rest mass energy, the resultant energy densities are approximately halved.

3 Gamma-ray data and constraints

Interstellar radiation field for inverse Compton scattering For inverse Compton cooling and emission calculations we assume the full interstellar radiation field determined for the inner 500 pc[62]. This has an energy density of ~ 19 eV cm^{-3}. Conservatively, we do not account for the growth in the energy density of the interstellar radiation field towards the GC (that would otherwise imply more inverse Compton emission).

Inverse Compton emission We calculate the Compton scattering emissivity of relativistic electrons using the full Klein-Nishina cross section[63].

Bremsstrahlung emission We use standard formulae[64] to calculate bremsstrahlung emission by relativistic electrons scattering on ambient hydrogen gas corrected (a multiplication by 1.4 given the 0.1 number fraction of He ions[30]) to account for the presence of heavier ions. We use the same cross-section in our treatment of both bremsstrahlung cooling and bremsstrahlung emission (so our treatment is self-consistent).

EGRET Constraint We claim a conservative upper limit to the integral intensity from the diffuse non-thermal source region of 1×10^{-4} cm^{-2} s^{-1} sr^{-1} above 300 MeV. This is obtained from figs. 2(c) and 2(d) of [65] which, when combined, show a pedestal in the super-300 MeV intensity. We estimate the pedestal intensity at $\sim 3 \times 10^{-4}$ cm^{-2} s^{-1} sr^{-1}, averaging over $|b| < 2^\circ$ and within the longitude defined by $|l| < 30^\circ$. Given that there are no structures evident in these longitude-dependent intensity plots on the size scale of the diffuse non-thermal source, we estimate an upper-limit to the diffuse non-thermal source intensity at the level of twice the largest actual excursion in the intensity above the pedestal value, viz. 1×10^{-4} cm^{-2} s^{-1} sr^{-1}. We are confident that a more detailed analysis would produce a more stringent constraint and thus rule out more of the magnetic field parameter space. In any case, results pertaining to the region from the Fermi (GLAST) telescope are eagerly awaited.

HESS Constraint Observations by the HESS instrument[59] proffer another, in-principle constraint on the (higher-energy members of the) same electron population of GC region responsible for the $\sim$GHz radio emission. This instrument has detected diffuse emission *over the smaller region* defined by $|l| < 0.8^\circ$ and $|b| < 0.3^\circ$ of 1.4×10^{-20} cm^{-2} eV^{-1} s^{-1} sr^{-1} (the solid angle denoted by the inner rectangle in fig. 1 of the main article) with only limited and dimmer diffuse TeV emission detected outside this region but within the diffuse non-thermal source field. With the raw count rate in the HESS signal region being only $\sim$ twice that in the background region (cf. [59], fig. 1b), the TeV intensity (within the rectangular region defined above) offers a conservative upper limit to the TeV γ-ray intensity of the diffuse non-thermal source region. As fig. 3 of the main article demonstrates, however, in reality this constraint is not particularly restrictive.

Broadband Spectrum We show an example broadband spectrum for a 100 μG field in fig. S7. The plot shows the bremsstrahlung (and, sub-dominantly, inverse Compton) emission from the very same electron population that is supplying the observed synchrotron radio signal.

4 Primary or Secondary Electrons?

That diffuse TeV γ-ray emission – likely attributable to the impacts of cosmic ray ions with ambient gas – has been detected within the diffuse non-thermal source[59] suggests that one consider the idea that *secondary* electron (+positron) synchrotron radiation contribute significantly to the observed, non-thermal radio spectrum. Here, such secondary electrons would be born in the decay chain of charged mesons, themselves created in the same cosmic ray ion impacts that (through the process of neutral meson decay) probably[59] lead to the observed $\sim$TeV emission.

We have considered such a scenario and find that, while in the absence of γ-ray constraints, a secondary electron model provides the best fit to the observed radio spectrum, once these are accounted for, such a model can be ruled out except for very high ($> 1000\mu$G) field amplitudes (see fig.S8). This does not, in itself, rule out the idea the secondaries supply much of the observed radio; rather, in the context of obtaining a lower limit to the actual field amplitude, a more conservative limit is obtained by hypothesizing that primary electrons supply the synchrotron flux density. The γ-ray limit is much more constraining for secondary electrons than for primary electrons because a neutral meson decay contribution to the γ-ray flux is only attendant upon the secondary production process.

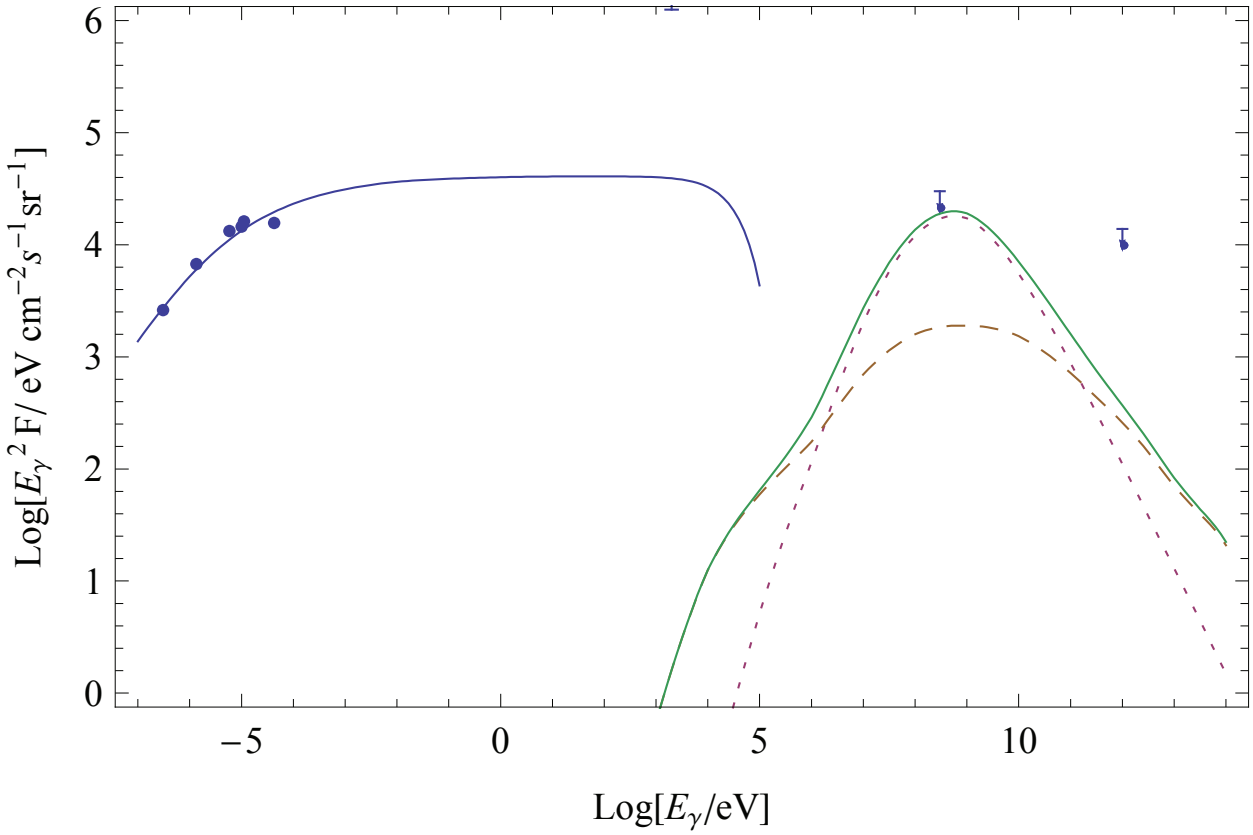

Figure S7: **Broadband spectrum of the diffuse non-thermal source region for magnetic field of 100 μG**. The injected electron spectrum is assumed to follow a power law (in momentum) up to $\sim$ 100 TeV. The lower energy blue curve is due to synchrotron emission. The higher energy curves are (dashed,brown) inverse Compton (IC), (dotted, purple) bremsstrahlung and (solid, green) combined IC+bremssrahlung. Note that for field amplitudes in the range 10-1000 μG, the electrons synchrotron radiating at $\sim$GHz frequencies are bremsstrahlung radiating at $\sim$GeV energies. The upper limits are due to observations by EGRET[65] at 300 MeV = 3×10^8 eV and HESS[59] at TeV = 10^{12} eV. The electron distribution is assumed to die off exponentially above an energy of 100 TeV.

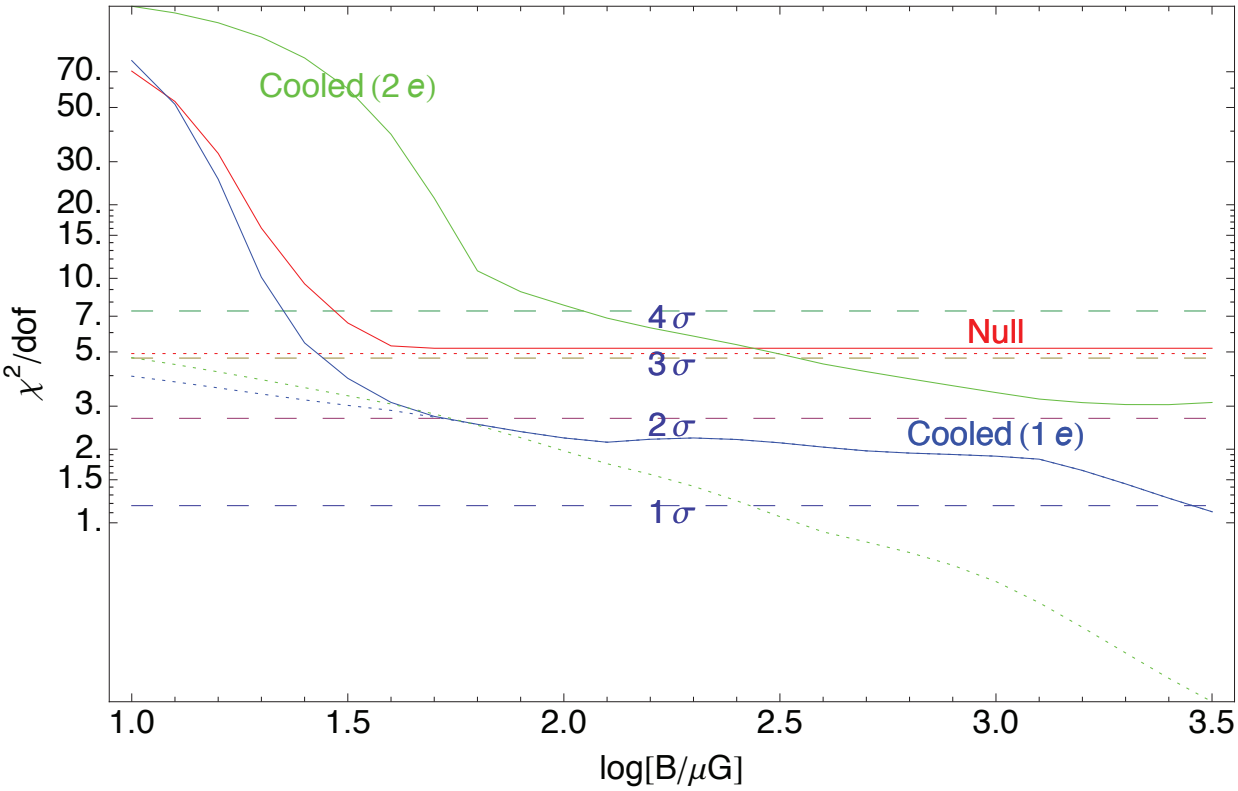

Figure S8: **Plot of the χ^2 per degree of freedom as a function of magnetic eld amplitude**. This is a reproduction of plot 1 from the main article showing, in addition, (in green) the χ^2 per degree of freedom as a function of magnetic field amplitude for a cooled *secondary* electron (+ positron) model. The solid green curve is constrained by the requirement that the bremsstrahlung and (sub-dominantly) inverse Compton emission, from the synchrotron-radiating *secondary* electron population *and* the inescapable addition contribution from neutral meson decay not over-produce 300 MeV γ-ray flux whereas the dotted green curve is not so constrained. The secondary electron model has the same number of degrees of freedom (3) as the primary electron model.

5 Inferred value of hydrogen number density

The best fit at our favoured field amplitude suggests an ambient hydrogen density where the electrons are radiating of $\sim 40\,\mathrm{cm}^{-3}$, only $\sim$3 times the volumetric average number density throughout the diffuse non-thermal source volume ($\sim 13\,\mathrm{cm}^{-3}$[30]) but much smaller than the density at which the typical GC hydrogen molecule finds itself which is $> 10^4\ \mathrm{cm}^{-3}$[32]. This may simply reflect that the relativistic particle population is fairly uniform across the region so that there are not large cosmic ray over-densities inside molecular clouds. Alternatively, this phenomenology is also consistent with a scenario[66] that sees cosmic rays accelerated diffusively in relatively tenuous GC interstellar medium phases before interacting primarily in the periphery of molecular clouds, possibly because neither primary electrons nor primary ions (that might generate synchrotron-radiating **secondary** electrons) can penetrate into dense cloud cores within the particles' loss times. Such a scenario is supported by recent work we have undertaken concerning the Sagittarius B Giant Molecular Cloud[58,67].

6 Far-infrared–radio continuum correlation and the diffuse non-thermal source

In useful units, the 1.4 GHz RC emission of the diffuse non-thermal source region is $\sim 3 \times 10^{19}$ Watt/Hz, whereas, on the basis of IRAS data[68] the 60 micron luminosity of the same region is $\sim 2 \times 10^8\,L_\odot$. These values place the diffuse non-thermal source within $\sim$0.5 dex (i.e., within $\sim 2\sigma$) of the empirical correlation of 1.4 GHz and the 60 micron luminosities determined[69] for a large sample of external galaxies.

7 Field required for hydrostatic equilibrium in the diffuse non-thermal source

The field required for hydrostatic equilibrium can be estimated as $2\sqrt{\Sigma_{gas}\Sigma_{tot}}$ mG where the gas and total surface mass densities are given in g cm^{-2} [70]. The average surface mass density in *gas* over the diffuse non-thermal source region can be estimated from ref [30] to be 0.01 g cm^{-2}. The *total* surface mass density – dominated by stars – is around 50 times[68] the gas surface density and hydrostatic equilibrium therefore requires a field of ~ 140 μG.

29. Morris, M., & Serabyn, E. The Galactic Center Environment, Ann. Rev. Astron. Astrophys., 34, 645-702 (1996)

30. Ferrière, K., Gillard, W., & Jean, P. Spatial distribution of interstellar gas in the innermost 3 kpc of our galaxy, Astron. Astrophys., 467, 611-627 (2007)

31. LaRosa, T. N. et al. Evidence of a Weak Galactic Center Magnetic Field from Diffuse Low-Frequency Nonthermal Radio Emission Astrophys. J., 626, L23-L27 (2005)

32. Paglione, T. A. D., Jackson, J. M., Bolatto, A. D., & Heyer, M. H. Interpreting the HCN/CO Intensity Ratio in the Galactic Center, Astrophys. J., 493, 680-693 (1998)

33. Higdon, J. C., Lingenfelter, R. E., & Rothschild, R. E. The Galactic Positron Annihilation Radiation & The Propagation of Positrons in the Interstellar Medium, Astrophys. J., 698, 350 (2009)

34. Revnivtsev, M., Sazonov, S., Churazov, E., Forman, W., Vikhlinin, A., & Sunyaev, R. Discrete sources as the origin of the Galactic X-ray ridge emission, Nature, 458, 1142-1144 (2009)

35. Güsten, R., & Philipp, S. D. Galactic Center Molecular Clouds, The Dense Interstellar Medium in Galaxies, Proceedings of the 4th Cologne-Bonn-Zermatt Symposium, Zermatt, Switzerland, 22-26 September 2003. Edited by S.Pfalzner, C. Kramer, C. Staubmeier, and A. Heithausen. Springer proceedings in physics, Vol. 91. Berlin, Heidelberg: Springer, 253-263 (2004) (astro-ph/0402019)

36. Miyazaki, A., & Tsuboi, M. Dense Molecular Clouds in the Galactic Center Region. II. Statistical Properties of the Galactic Center Molecular Clouds, Astrophys. J., 536, 357-367 (2000)

37. Cooper, B. F. C., & Price, R. M. A high resolution survey of the Galactic Centre region and spectral characteristics of the region, The Galaxy and the Magellanic Clouds, 20, 168-172 (1964)

38. Ekers, R. D., & Lynden-Bell, D. High Resolution Observations of the Galactic Center at 5 GHz, Astrophysical Letters, 9, 189–193 (1971)

39. Whiteoak, J. B., & Gardner, F. F. A 5-GHz Survey of the Galactic Center Region with a Resolution of 4 arc min Astrophysical Letters, 13, 205–207 (1973)

40. LaRosa, T. N., Kassim, N. E., Lazio, T. J. W., & Hyman, S. D. A Wide-Field 90 Centimeter VLA Image of the Galactic Center Region, Astronom.J., 119, 207-240 (2000)

41. Reich, W., Reich, P., Fuerst, E. The Effelsberg 21 CM radio continuum survey of the Galactic plane between L = 357 deg and L = 95.5 deg, Astron. Astrophys., Suppl.,83, 539-568 (1990)

42. Duncan, A.R., et al. A deep radio continuum survey of the southern Galactic plane at 2.4 GHz, Mon. Not. Roy. Astron. Soc., 277, 36-52 (1995)

43. Reich, W., Fuerst. E., Steffen, P., Reif, K., Haslam, C.G.T. A radio continuum survey of the Galactic Plane at 11 CM wavelength. I - The area L = 357.4 to 76 deg, B = -1.5 to +1.5 deg, Astron. Astrophys., Suppl., 58, 197-248 (1984)

44. Langston, G. et al. The First Galactic Plane Survey at 8.35 and 14.35 GHZ, Astron. J., 119, 2801-2827 (2000)

45. Handa, T. et al. A radio continuum survey of the Galactic plane at 10 GHz, Proc. Astron. Soc. Jap., 39, 709-753 (1987)

46. Finkbeiner, D. P. et al. Microwave Interstellar Medium Emission in the Green Bank Galactic Plane Survey: Evidence for Spinning Dust, Astrophys. J., 617, 350-359 (2004)

47. Crovisier, J., & Dickey, J. M. The spatial power spectrum of galactic neutral hydrogen from observations of the 21-cm emission line, Astron. Astrophys., 122, 282-296 (1983)

48. Dickey, J.M., McClure-Griffiths, N.M., Stanimirovic, S., et al. Southern Galactic Plane Survey Measurements of the Spatial Power Spectrum of Interstellar H I in the Inner Galaxy, Astrophys. J., 561, 264-271 (2001)

49. Schmidt, J. 1978, PhD dissertation, University of Bonn

50. Law, C. J., Yusef-Zadeh, F., Cotton, W. D., & Maddalena, R. J. Green Bank Telescope Multi-wavelength Survey of the Galactic Center Region, Astrophys.J.Suppl., 177, 255-274 (2008)

51. Haslam, C.G.T. et al. A 408 MHz all-sky continuum survey. II - The atlas of contour maps, Astron. Astrophys. Supp., 47, 1-142 (1982)

52. Platania, P. et al. Full sky study of diffuse Galactic emission at decimeter wavelengths, Astron. Astrophys., 410, 847-863 (2003)

53. Voelk, H. J. The correlation between radio and far infrared emission for disk galaxies: a calorimeter theory, Astron. Astrophys., 218, 67-70 (1989)

54. Stanimirovic, S., *ASP Conference Series: Single-Dish Radio Astronomy: Techniques and Applications*, Eds. Stanimirovic, S., Altschuler, D.R., Goldsmith, P.F. & Salter, C.J., ASP Conference Proceedings, Vol. 278, ISBN: 1-58381-120-6. San Francisco: Astronomical Society of the Pacific, (2002).

55. Sofue, Y., & Reich, W. Radio continuum observations of the North Polar Spur at 1420 MHz, Astron. Astrophys. Supp., 38, 251-263 (1979)

56. Haynes, R.F., Stewart, R.T., Gray, A.D., et al. Polarized arcs near the Galactic Centre, Astron. Astrophys., 264, 500-512 (1992)

57. Sofue, Y., Takahara, F., Hirabayashi, H., et al. 10-GHz observations of the unusual supernova remnant CTB80 associated with jet-like features, Proc. Astron. Soc. Jap., 35, 437-445 (1983)

58. Crocker, R. M., et al. The Cosmic Ray Distribution in Sagittarius B Astrophys. J., 666, 934-948 (2007)

59. Aharonian, F. A. et al. Discovery of very-high-energy γ-rays from the Galactic Centre ridge, Nature, 439, 695-698 (2006)

60. Figer, D., et al. An Extended Star Formation History for the Galactic Center from Hubble Space Telescope NICMOS Observations, Astrophys. J., 601, 319-339 (2004)

61. Belmont, R., et al. A Hot Helium Plasma in the Galactic Center Region, Astrophys. J.631, 53-56 (2005)

62. Porter, T. A., Moskalenko, I. V., & Strong, A. W. Inverse Compton Emission from Galactic Supernova Remnants: Effect of the Interstellar Radiation Field, Astrophys. J., 648, L29-L32 (2006)

63. Sturner, S. J. et al. Temporal Evolution of Nonthermal Spectra from Supernova Remnants, Astrophys. J., 490, 619-632 (1997)

64. Baring, M. G., et al. Radio to Gamma-Ray Emission from Shell-Type Supernova Remnants: Predictions from Nonlinear Shock Acceleration Models, Astrophys. J., 513, 311-338 (1999)

65. Hunter, S. D., et al. EGRET Observations of the Diffuse Gamma-Ray Emission from the Galactic Plane, Astrophys. J., 481, 205-240 (1997)

66. Wommer, E., Melia, F., & Fatuzzo, M. Diffuse TeV emission at the Galactic Centre, Mon. Not. Roy. Astron. Soc., 387, 987-997 (2008)

67. Protheroe, R. J., Ott, J., Ekers, R. D., Jones, D. I., & Crocker, R. M. Interpretation of radio continuum and molecular line observations of Sgr B2: free-free and synchrotron emission, and implications for cosmic rays, Mon. Not. Roy. Astron. Soc.390, 683-692 (2008)

68. Launhardt, R., Zylka, R., & Mezger, P. G. The nuclear bulge of the Galaxy I I I. Large-scale physical characteristics of stars and interstellar matter, Astron. Astrophys., 384, 112-139 (2002)

69. Yun, M. S., Reddy, N. A., & Condon, J. J. Radio Properties of Infrared-selected Galaxies in the IRAS 2 Jy Sample, Astrophys. J., 554, 803-822 (2001)

70. Thompson, T. A., Quataert, E., Waxman, E., Murray, N., & Martin, C. L. Magnetic Fields in Starburst Galaxies and the Origin of the FIR-Radio Correlation, Astrophys. J., 645, 186-198 (2006)